CrystEngComm

Accepted Manuscript

ROYAL SOCIETY OF CHEMISTRY

www.rsc.org/crystengcomm

Journal Name

RSCPublishing

COMMUNICATION

Template-free preparation of mesoporous g-C_3N_4/TiO_2 nanocomposite photocatalyst and its properties

Cite this: DOI: 10.1039/x0xx00000x

Jianchao Shen,[a] Hui Yang,[a, b] Qianhong Shen,[*a, b] Yu Feng,[a] and Qifeng Cai [a]

Received 00th January 2012,
Accepted 00th January 2012

DOI: 10.1039/x0xx00000x

www.rsc.org/

Abstract: A novel and facile template-free method was presented to fabricate a network structured mesoporous g-C_3N_4/TiO_2 nanocomposite with enhanced visible-light photocatalytic activities. The protonation effect accompanied with TiO_2 nanoparticle growth is believed to be a probable mechanism for the formation of such pore structure in g-C_3N_4 matrix.

Graphitic carbon nitride (g-C_3N_4), as a novel visible light driven metal-free photocatalyst, has stimulated intensive interest in the photocatalytic field due to its high stability, appealing electronic structure and medium band gap [1]. However, the photocatalytic activity of the bulk g-C_3N_4 is limited by its low specific surface area and poor quantum yield, so a number of strategies have been employed to modify bulk g-C_3N_4 [2].

To increase specific surface area and thus providing more active sites for adsorption and photocatalytic reaction, various soft or hard templates are usually employed to introduce pores in g-C_3N_4 [3]. The pores can be fabricated after the removal of templates, but this extra template removal step may induce adverse impact on the preparation and properties of as-prepared g-C_3N_4. For example, the most used hard templates of porous silicas are usually removed by dissolving in NH_4HF_2, HF or NaOH aqueous solutions, which are not environmentally friendly [4]. While for the soft templates, such as a variety of surfactants and amphiphilic block polymers, it is difficult to avoid the increase of carbon content in the resulting materials as well as the generation of more potential recombination centers in semiconductors, which will lead to the decrease of photocatalytic activity [5]. Therefore, the developments of new procedures for synthesizing porous g-C_3N_4 without templates are of particular interest. Recently, it is reported that the direct protonation of the base functionalities in g-C_3N_4 can make bulk g-C_3N_4 be broken up from its defects, thereby forming the relatively fine fragment particles [6]. This strategy has provided a convenient route to raise the specific surface area of bulk g-C_3N_4.

On the other hand, to increase the quantum yield of g-C_3N_4, many methods have been developed to inhibit the recombination of photo-generated electron-hole pairs, such as doping with foreign elements [7], and coupling with graphene [8], noble metal [9] or other semiconductors [10]. Among them, coupling g-C_3N_4 with other

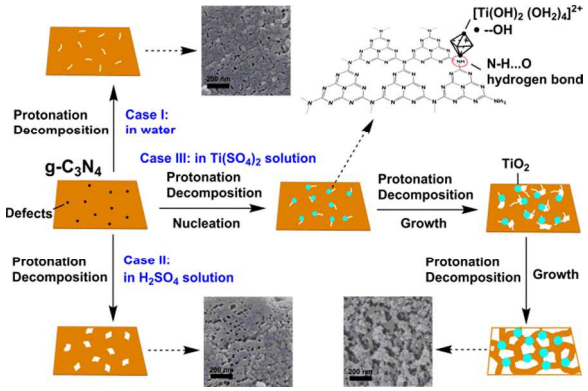

Scheme. 1 Formation mechanism of various modified g-C_3N_4 samples.

components is a promising strategy for improving the charge separation in photocatalysis, especially when the nanojunction structure is formed in the composites, which will promote a more efficient interparticle electron transfer due to the size effect of particles and intimate contact between heterophase nanoparticles [10].

In this communication, we report a novel and facile chemical method to fabricate a mesoporous g-C_3N_4/TiO_2 nanocomposite based on the protonation of base functionalities as well as the in situ growth of TiO_2 nanoparticles on g-C_3N_4 surface. The as-prepared g-C_3N_4/TiO_2 nanocomposite exhibits efficient interparticle electron transfer, achieving the enhanced quantum efficiency. More interestingly, the protonation effect induces forming unexpected network structured mesopores in the bulk g-C_3N_4 rather than obtaining fine fragment g-C_3N_4 particles [6]. To the best of our knowledge, this work is the first report of such phenomenon, and also provides a new idea for preparing mesoporous g-C_3N_4 based materials through template-free route.

To understand the formation mechanism of mesoporous g-C_3N_4/TiO_2 (denoted as CN-Ti), the pure g-C_3N_4 modified in the ethanol-water solution (denoted as CN-H) and H_2SO_4 solution (denoted as CN-S when the solution has the same pH value as that of the g-C_3N_4/TiO_2 preparation system, and CN-SS when the solution

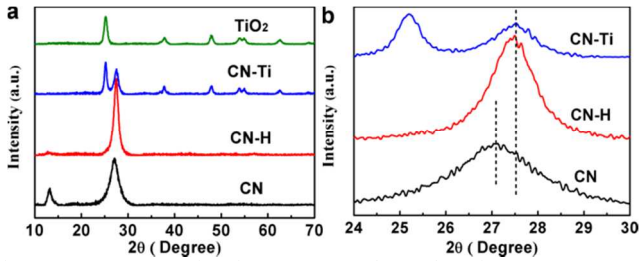

Fig. 1 XRD patterns of various as-prepared samples of CN, CN-H, CN-Ti and TiO_2 in the range of (a) 2θ = 10º-70º; (b) 2θ = 24º-30º.

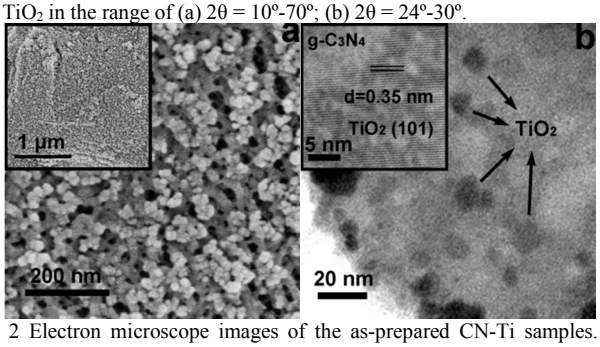

Fig. 2 Electron microscope images of the as-prepared CN-Ti samples. (a) SEM image, and the inset is the corresponding image of low magnification. (b) TEM image, and the inset is the corresponding image of high resolution.

has even lower pH value) were also prepared by the similar procedure for reference, respectively. The formation mechanism of various modified g-C_3N_4 samples are illustrated in Scheme. 1.

Under the hydrothermal conditions, the water has higher reaction activity than itself in normal state due to the increase of its self-ionization constant, leading to the protonation of base functionalities in g-C_3N_4 (Case I in Scheme. 1). As shown in Fig. 1a, the diffraction peak of the pure g-C_3N_4 without modification (denoted as CN) at 2θ=13.1°, which represents the in-plane structural packing motif, disappears after the hydrothermal reaction, indicating that the protonation occurs [6]. Moreover, the diffraction peak of CN sample at 2θ=27.1° shifts to higher angles in the XRD pattern of CN-H sample due to modified interlayer organization, accompanied by a compression of the average interlayer distance towards smaller d values (Fig. 1b) [11]. Owing to the protonation effect, the g-C_3N_4 will decompose to clusters/oligomers of condensed triazine-rings [6]. As a result, parts of the clusters/oligomers with well water-solubility will be removed by decomposition under hydrothermal conditions, forming some sporadic pores and cracks on the surface of CN-H sample [12] (Fig. S1b, ESI†). Furthermore, when modifying the g-C_3N_4 in H_2SO_4 solution (Case II in Scheme. 1), which has the same pH value as that of the g-C_3N_4/TiO_2 preparation system, the water-soluble clusters/ oligomers may increase due to the more intense protonation effect at higher proton concentration, so the porosity of CN-S sample is increased (Fig. S1c, ESI†). Actually, when further increasing H_2SO_4 dosage in reaction system, the porosity of g-C_3N_4 will be increased more obviously, further confirming the promotion effect of protonation on the formation of mesoporous structure (Fig. S1d, ESI†).

However, when introducing $Ti(SO_4)_2$ as the precursor of TiO_2 (Case III in Scheme. 1), a network porous structure appears in g-C_3N_4 matrix, which is quite different from that of CN-S sample although they have the same preparation condition of pH value (Fig. 2a). At the beginning of the hydrothermal reaction, the intense protonation will occur in the presence of H_2SO_4, which is generated from the hydrolysis of $Ti(SO_4)_2$, leading to the formation of some little pores and microcracks, thereby increasing the defects on the surface of g-C_3N_4. Meanwhile, in a low concentration aqueous $Ti(SO_4)_2$ solution, Ti^{4+} exists as an octahedral $[Ti(OH)_2(OH_2)_4]^{2+}$

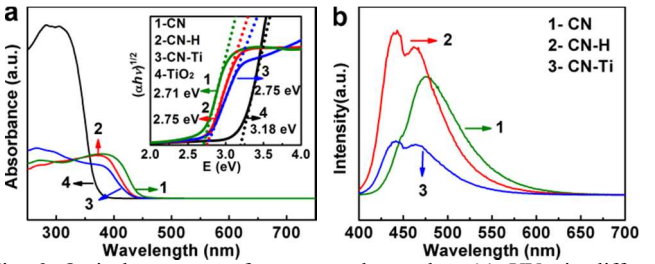

Fig. 3 Optical property of as-prepared samples. (a) UV–vis diffuse reflectance spectra of various samples. The inset is the band gap of as-obtained samples determined from the $(\alpha h\nu)^{1/2}$ versus photon-energy plots. (b) PL emission spectra of various samples monitored at an excitation wavelength of 325 nm.

monomer or an edge-sharing dimmer [13]. The g-C_3N_4 is favorable to the adsorption of $[Ti(OH)_2(OH_2)_4]^{2+}$ species on the formed g-C_3N_4 surface defects of terminal amino groups or bridging nitrogens via hydrogen bonding force [14], thus providing the nucleating sites for the growth of TiO_2 nanocrystals. With the hydrothermal reaction proceeds, the solution is in a saturated state, and the $[Ti(OH)_2(OH_2)_4]^{2+}$ species in solution are unstable and prone to combine together through oxolation or olation at the nucleating sites to form original nuclei, and then the nuclei grow further into anatase type crystallites (Fig. 1 and Fig. 2) [13]. The increasing particle size of TiO_2 nanoparticles at the formed defects, such as little pores and microcracks, may result in the increase of tensile stress on the surface of g-C_3N_4, and thus forming more cracks. Therefore, more protons will diffuse into the inner layer of g-C_3N_4 through the new formed cracks, inducing a new round of the protonation and decomposition. Finally, the network mesoporous structure is formed, and the specific surface area is increased from 3.53 $m^2\ g^{-1}$ to 21.21 $m^2\ g^{-1}$ (Fig. S2, ESI†). According to the results of particle size distribution (Fig. S3, ESI†), the increase of specific surface area is mainly caused by the network mesporous structure rather than g-C_3N_4 particle refinement. Furthermore, the typical layered structure of g-C_3N_4, as well as melem structure acting as a visible-light sensitizer [15], is well kept after the intense protonation, and the obtained CN-Ti sample contains two fundamental components of g-C_3N_4 and anatase TiO_2 (Fig. 1 and Fig. S4, ESI†). These two components have formed a close interface (Fig. 2b), which is favorable for the highly efficient interparticle electron transfer.

Fig. 3a shows UV-vis diffuse reflectance spectra of as-prepared samples. It can be seen that the CN sample exhibits an intrinsic semiconductor-like absorption in the blue region of visible spectrum with band edge wavelength around 458 nm. The UV-vis diffuse reflectance spectrum of CN-H sample indicates that the optical band gap and the semiconductor properties are maintained, while the band edge wavelength blue shifts from 458 nm to 451 nm. After combining g-C_3N_4 with TiO_2, the optical absorption of CN-Ti sample is decreased slightly in the region of 350 - 450 nm, while enhanced in the region of ultraviolet light below 330 nm. This phenomenon can be contributed to optical response of TiO_2 and g-C_3N_4 as well as the combination of these two semiconductors. Furthermore, the band gap determined from the $(\alpha h\nu)^{1/2}$ versus photon-energy plots are about 2.71 eV(CN), 2.75 eV (CN-H), 2.75 eV (CH-Ti), 3.18 eV (TiO_2), respectively. Fig. 3b illustrates PL emission spectra of as-prepared samples monitored at an excitation wavelength of 325 nm. The CN sample shows a typical PL spectrum with the emission peak at 475 nm. However, the PL curve of CN-H sample is splitted into two peaks with the emission peak around 440 nm and 460 nm, and the fluorescence intensity is increased compared with CN sample. This phenomenon is believed to be a result of the protonation of base functionalities in g-C_3N_4 [6]. After introducing TiO_2 nanoparticles on the surface of g-C_3N_4, the

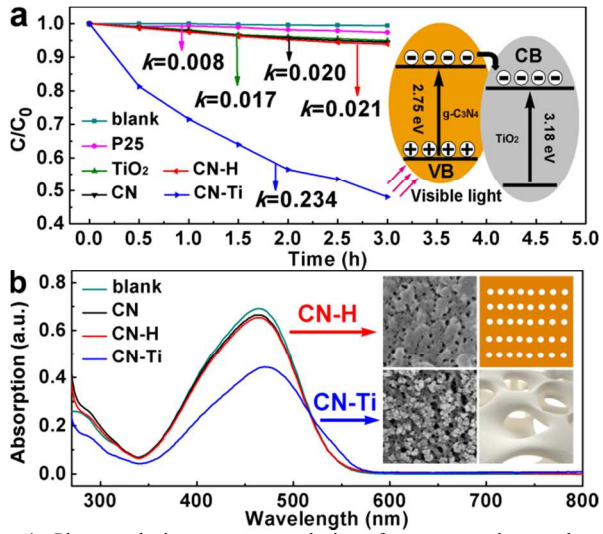

Fig. 4 Photocatalysis process analysis of as-prepared samples. (a) Phohotocatalytic degradation and corresponding kinetics of MO over P25 particles and as-prepared samples of TiO_2, CN, CN-H, CN-Ti under visible-light irradiation. The inset shows the proposed electron-hole separation process of g-C_3N_4/TiO_2 nanojunction under visible-light irradiation. (b) UV-vis spectra of MO after absorption by the CN, CN-H and CN-Ti sample in the dark for 2h. The inset displays the corresponding surface structure of CN-H and CN-Ti sample.

fluorescence intensity of CN-Ti sample is significantly reduced, indicating that the recombination of photo-generated charge carriers is greatly inhibited due to the efficient electron transfer between g-C_3N_4 and TiO_2. This result shows good agreement with other heterojunction semiconductors [10].

The photocatalytic performance of as-prepared samples are evaluated by methyl orange (MO) photocatalytic degradation under visible-light ($\lambda > 420$ nm) irradiation. The corresponding first-order kinetics plot by the equation of $\ln(C_0/C) = kt$ is shown in Fig. 4a, where C_0 and C are the MO concentrations in solution at times 0 and t, respectively, and k is the apparent first-order rate constant. It can be seen that the commercial P25 and as-prepared TiO_2 show rather weak activities as they work only with ultraviolet irradiation, while CN-Ti sample exhibits an excellent photocatalytic degradation rate of 0.234 h^{-1}, which is about as 29.3, 13.8, 11.7 and 11.4 times high as that of P25, TiO_2, CN and CN-H sample, respectively. As discussed above, CN-Ti sample shows much higher specific surface area than that of other samples else, and becomes positively charged due to the protonation, thereby inducing higher adsorption capacity to negatively charged MO molecules (Fig. 4b).

Fig. 5a illustrates UV-vis absorption spectra of MO solution photocatalytic degraded by CN-Ti sample for different time intervals under visible light. It can be seen that the characteristic absorption peak of the initial MO solution at 464 nm, which is associated with the azo bond (–N=N–) [16], shows a large decrease in intensity simultaneously with a significant blue shift during photocatalysis process, resulting in the distinct color change from orange to light yellow-green. By the means of peak fitting, the broadened absorption peak can be further devided into three peaks located at 464nm, 438 nm and 380 nm (the inset of Fig. 5a). This suggests that some intermediates may be generated, and the color of the resulting solution changes as a result of the competition between degradation of MO chromophore ring and production of the intermediates. The resulting solutions from photocatalytic degradation are further analyzed by using HPLC, as shown in Fig. 5b. There can be found a fast intensity decrease of MO peak at 8.5 min and the appearance of two new peaks emerged at retention times of 6.7 (IM1) and 4.3 (IM2)

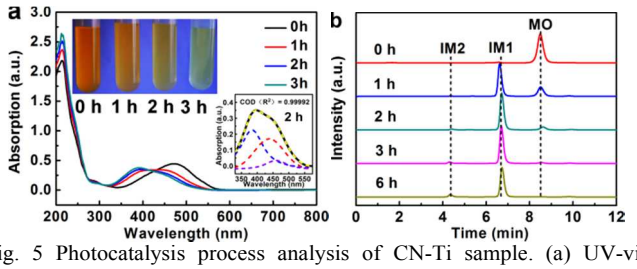

Fig. 5 Photocatalysis process analysis of CN-Ti sample. (a) UV-vis spectra of MO solution photocatalytic degraded by CN-Ti sample for different time intervals under visible light. The insets show the color change of corresponding resulting solution and peak fitting of a typical UV-vis absorption spectrum of the resulting solution after 2 h irradiation. (b) The HPLC chromatograms of MO solution photocatalytic degraded by CN-Ti sample for different time intervals under visible light.

min, respectively. This result further confirms the generation of intermediates during the photocatalytic degradation.

Indeed, the N-demethylation of MO will occur due to the attack of hydroxyl radicals on the N,N-dimethyl groups, generating aminoazobenzene-4'-sulfonic acid sodium salt [17], which corresponds to the IM1 peak in the HPLC chromatogram. Therefore, with the photocatalytic reaction proceeds, IM1 peak increases gradually with the decrease of MO in the initial 3 hours, resulting in the blue shift of main absorption peak position from 464 nm to 438 nm in UV-Vis spectra. Subsequently, the aminoazobenzene-4'-sulfonic acid sodium salt will be further oxidized by hydroxyl radicals, producing p-nitroaniline due to the cleavage of azo-bond. The p-nitroaniline has characteristic UV-vis absorption peak at 380 nm [18], which is in well agreement with the analysis of peak fitting. Considering the molecule polarity and the response characteristic under the detection wavelength of HPLC, the small peak at 4.5 min, which is obviously increased with the decrease of IM1 peak after photocatalytic reaction for 6 h, may attribute to p-nitroaniline. Hence, it can be speculated that the possible photocatalytic degradation pathway for MO in this reaction system involves N-demethylation of MO to generate aminoazobenzene-4'-sulfonic acid sodium salt, followed by cleavage of the azo-bond to yield kinds of intermediates [19].

Based on above discussion and analysis, the highly efficient photocatalytic activity are mainly ascribed to the following two aspects: on the one hand, owing to the delocalized conjugated π structure of g-C_3N_4, coupling it with the wide band gap TiO_2 is a suitable approach to achieve an improved charge separation [10] (The inset of Fig. 4a), thereby increasing yield of hydroxyl radicals, which play a crucial role for photocatalytic reaction in presence of g-C_3N_4 based photocatalyst [20]. On the other hand, the network mesoporous structure in CN-Ti sample will improve adsorption capacity for the target pollutants and provide more active sites to accelerate the photocatalytic degradation [3]. Therefore, as-prepared mesoporous g-C_3N_4/TiO_2 nanocomposite exhibits highly efficient photocatalytic activity under visible light.

Conclusions

The conclusions section should come at the end of the article. In summary, we developed a novel and facile template-free method to fabricate the mesoporous g-C_3N_4 based material. Protonation of base functionalities lets g-C_3N_4 decompose to clusters/oligomers of condensed triazine-rings, some of which with well water-solubility can be removed under hydrothermal conditions. Moreover, the in situ growth of TiO_2 nanoparticles on the surface of g-C_3N_4 not only forms g-C_3N_4/TiO_2 nanojunction with more efficient interparticle electron transfer, but also promotes the further protonation, thereby increasing

the porosity of g-C_3N_4 matrix. As-prepared mesoporous g-C_3N_4/TiO_2 nanocomposite combined the advantages of visible-light response, efficient charge separation and high adsorption ability for contaminant molecule, thus exhibiting highly efficient photocatalytic activity under visible light. Works focused on the performance optimization of this functionalized g-C_3N_4 and coupling g-C_3N_4 with other semiconductors are ongoing.

We would like to thank Key Technologies R&D Program of China under Grant No.2013BAJ10B05, Zhejiang Provincial Natural Science Foundation of China under Grant No.LQ12E02008 and Fundamental Research Funds for the Central Universities under Grant No.ZJUR011104.

Notes and references

[a] *State Key Laboratory of Silicon Materials, Department of Materials Science & Engineering, Zhejiang University, Hangzhou 310027, P. R. China. E-mail: s_qianhong@163.com; Fax: +86 571 87953313; Tel: +86 0571 87953313*

[b] *Zhejiang California International NanoSystems Institute, Zhejiang University, Hangzhou 310027, P. R. China*

† Electronic Supplementary Information (ESI) available: See DOI: 10.1039/c000000x/

1 (a) X. Wang, K. Maeda, A. Thomas, K. Takanabe, G. Xin, J. M. Carlsson, K. Domen and M. Antonietti, *Nat. Mater.*, 2009, **8**, 76; (b) X. H. Li, X. Wang and M. Antonietti, *Chem. Sci.*, 2012, **3**, 2170.

2 (a) X. Bai, L. Wang, R. Zong and Y. Zhu, *J. Phys. Chem. C*, 2013, **117**, 9952; (b) Y. Wang, Z. Wang, S. Muhammad and J. He, *CrystEngComm*, 2012, **14**, 5065.

3 (a) F. Su, S. C. Mathew, G. Lipner, X. Fu, M. Antonietti, S. Blechert and X. Wang, *J. Am. Chem. Soc.*, 2010, **132**, 16299; (b) S. Yang, W. Zhou, C. Ge, X. Liu, Y. Fang and Z. Li, *RSC Adv.*, 2013, **3**, 5631; (c) H. Yan, *Chem. Commun.*, 2012, **48**, 3430.

4 (a) F. Goettmann, A. Fischer, M. Antonietti and A. Thomas, *Angew. Chem. Int. Ed.*, 2006, **45**, 4467; (b) X. Wang, K. Maeda, X. Chen, K. Takanabe, K. Domen, Y. Hou, X. Fu and M. Antonietti, *J. Am. Chem. Soc.*, 2009, **131**, 1680.

5 Y. Wang, X. C. Wang, M. Antonietti and Y. J. Zhang, *ChemSusChem*, 2010, **3**, 435.

6 Y. Zhang, A. Thomas, M. Antonietti and X. Wang, *J. Am. Chem. Soc.*, 2009, **131**, 50.

7 (a) J. Li, B. Shen, Z. Hong, B. Lin, B. Gao and Y. Chen, *Chem. Commun.*, 2012, **48**, 12017; (b) Y. J. Zhang, T. Mori, J. H. Ye and M. Antonietti, *J. Am. Chem. Soc.*, 2010, **132**, 6294.

8 Q. Xiang, J. Yu and M. Jaroniec, *J. Phys. Chem. C*, 2011, **115**, 7355.

9 L.Ge, C. Han, J. Liu and Y. Li, *Appl. Catal. A: Gen.*, 2011, **409-410**, 215.

10 (a) S. Kumar, T. Surendar, A. Baruah and V. Shanker, *J. Mater. Chem. A*, 2013, **1**, 5333; (b) S. C. Yan, S. B. Lv, Z. S. Li and Z. G. Zou, *Dalton Trans.*, 2010, **39**, 1488.

11 A. Thomas, A. Fischer, F. Goettmann, M. Antonietti, J. Müller, R. Schlögl and J. M. Carlsson, *J. Mater. Chem.*, 2008, **18**, 4893.

12 M. Shahbaz, S. Urano, P. R. LeBreton, M. A. Rossman, R. S. Hosmane and N. J. Leonard, *J. Am. Chem. Soc.*, 1984, **106**, 2805.

13 Y. Zheng, E. Shi, Z. Chen, W. Li and X. Hu, *J. Mater. Chem.*, 2001, **11**, 1547.

14 T. Saplinova, V. Bakumov, T. Gmeiner, J. Wagler, M. Schwarz and E. Kroke, *Z. Anorg. Allg. Chem.*, 2009, **635**, 2480.

15 D. Mitoraj and H. Kisch, *Angew. Chem. Int. Ed.*, 2008, **47**, 9975.

16 M. Hou, F. Li, X. Liu, X. Wang and H. Wan, *J. Hazard. Mater.*, 2007, **145**, 305.

17 C. Galindo, P. Jacques and A. Kalt, *J. Photoch. Photobio. A*, 2000, **130**, 35.

18 C. Y. Chiu, P. J. Chung, K. U. Lao, C. W. Liao and M. H. Huang, *J. Phys. Chem. C*, 2012, **116**, 23757.

19 J. R. Darwent and A. Lepre, *J. Chem. Soc., Faraday Trans. 2*, 1986, **82**, 1457.

20 S. C. Yan, Z. S. Li and Z. G. Zou, *Langmuir*, 2009, **25**, 10397.

A facile template-free method was proposed to fabricate a novel network structured mesoporous g-C_3N_4/TiO_2 nano-heterojunction composite via protonation of base functionalities during the in situ growth of TiO_2 nanoparticles on the surface of g-C_3N_4 under hydrothermal conditions.